Analytica Chimica Acta 1195 (2022) 339442

Contents lists available at ScienceDirect

Analytica Chimica Acta

journal homepage: www.elsevier.com/locate/aca

Sensory analysis of hepatitis B virus DNA for medicinal clinical diagnostics based on molybdenum doped ZnO nanowires field effect transistor biosensor; a comparative study to PCR test results

Mohsen Shariati [a], Mahdi Sadeghi [a, *], S.H. Reza Shojaei [b]

[a] Medical Physics Department, School of Medicine, Iran University of Medical Sciences, P.O. Box, 14155-6183, Tehran, Iran
[b] Department of Physics, Faculty of Science, Sahand University of Technology, Tabriz, Iran

HIGHLIGHTS

- A FET biosensor based on Mo doped ZnO NWs for HBV detection in label free was reported.
- Complementary DNA target was diagnosed in concentration ranges from 1 pM to 10 μM.
- Sensitivity response of the HBV biosensor showed a limit of detection (LOD) of 1 pM.
- Biosensor could distinguish the clinical samples TP, TN, FP and FN from each other.
- Results showed that the FET biosensor had better response in comparison to PCR test.

GRAPHICAL ABSTRACT

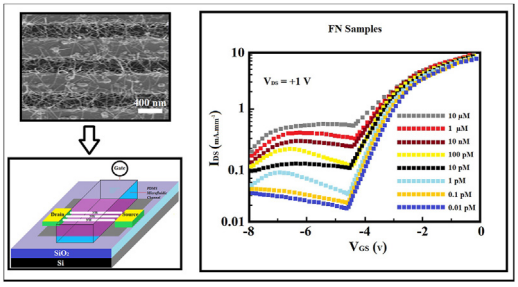

ARTICLE INFO

Article history:
Received 18 October 2021
Received in revised form
13 December 2021
Accepted 3 January 2022
Available online 5 January 2022

Keywords:
Biosensor
Hepatitis B Virus
Molybdenum doped ZnO Nanowires
Field-effect transistor
Label-free mechanism

ABSTRACT

In this paper, a bio-sensing setup for investigating hepatitis B virus deoxyribonucleic acid (HBV DNA) diagnosis including rapid testing and field effect transistor (FET) in label free assay is proposed. The FET biosensor was fabricated by molybdenum doped ZnO nanowires (NWs) in easy method and cost-free approach. The materialized NWs were synthesized by physical vapor deposition (PVD) growth mechanism. The molybdenum dopant could bring about vacancy sites for DNA adsorption and electric charge transfer. The capability of the fabricated biosensor was evaluated by investigating the PCR-verified samples known as True Positive (TP), True Negative (TN), False Positive (FP) and False Negative (FN). The FET biosensor could materialize the clinical tests on samples TP, TN, FP and FN and could distinguish the clinical samples from each other. The designed biosensor showed more precision than the PCR-outcomes by exhibiting more sensitivity on labeled samples known as FN. This research has analytical and comparative study on fabricated biosensor performance. The achieved results show that the biosensor had significant response to samples which have not been carefully detected by PCR test. The fabricated biosensor showed high accuracy, precision, sensitivity, specificity and reproducibility for differentiating (TP), (TN), (FP) and (FN) samples from healthy and normal sample. The response sensitivity was calculated and biosensor showed a detection limit (LOD) of 1 pM. The biosensor demonstrated high response and satisfied signal in the concentration ranges from 1 pM to 10 μM.

* Corresponding author.
E-mail address: sadeghi.m@iums.ac.ir (M. Sadeghi).

https://doi.org/10.1016/j.aca.2022.339442
0003-2670/

1. Introduction

Hepatitis B virus (HBV) is a small DNA virus in the family Hepanaviridae [1]. The virus is a major cause of hepatitis, including acute hepatitis, chronic hepatitis, cirrhosis and hepatocellular carcinoma (HCC) [1]. Although the vaccine is used to prevent the spread of the hepatitis B virus, new patients become infected each year [2]. In 2015, the World Health Organization (WHO) announced that 900,000 people worldwide had died from the effects of hepatitis infection [2]. Therefore, if an effective and rapid method of diagnosing hepatitis B is available, it will prevent the spread and control the transmission of the disease, [3].

A large number of efforts for HBV detection have been materialized [4]. A novel biosensor for detection of a single-nucleotide polymorphism related to the HBV based on HRCA was fabricated. The enhanced fluorescence intensity could detect the analyte [3]. Hepatitis B virus was detected through tin-doped WO_3/In_2O_3 NWs hetero-junction photo-electrode. The photo-electrode via the electrochemical impedance responses (EIS) could detect the hybridization of complementary HBV [5]. A HBV DNA biosensor based on gold nanocrystals (AuNCs) was operated through EIS approach under redox reactions process. The selectivity was investigated and the results were coincided with distinguishability of 1-, 2- and 3-mismatch targets [6]. A FET HBV DNA biosensor based on ITO NWs was fabricated. The fabricated biosensor could detect single-stranded hepatitis B virus DNA (SS-DNA) and diagnosed the target after hybridization of SS-DNA with complementary oligonucleotides [7].

Several methods and bio-sensing system were developed for HBV detection [4]. Among detection system, the FET-based biosensors have been used in wide fields especially in analyte detection [8,9]. These devices would allow the label-free detection of bio-molecules by measuring their intrinsic charges [10]. The detection limit of these sensors was determined by the Debye screening of the charges from counter ions in solutions [8–13].

As the building blocks for FET-based biosensors, one-dimensional ZnO nanostructures offer excellent surface-to-volume ratio and are more suitable and sensitive for sensing applications [14]. During the past decade, ZnO nanostructures FET-based biosensors are smartly designed and used due to their great specificity, sensitivity, and high selectivity [14]. Additionally, they have the advantage of low weight, low cost of mass production, small size and compatible with commercial planar processes for large-scale circuitry and biomolecule detection i.e. glucose, cholesterol, uric acid, urea, hormone, proteins, nucleotide, biomarkers [14]. The selective detection of multi-ions with ZnO nanorods FETs array sensor for detecting wide linear ranges of PO_4^{-3}, NO_3^-, and K^+ ions has been reported [15]. The fabrication of vertically oriented ZnO nanosheets based solution-gated field-effect transistor (FET) sensor for the low concentration detection of hydrazine has been reported [16]. The conductance of the solution-gated FET hydrazine sensor showed substantial change upon addition of different concentrations of hydrazine [16]. The fabrication of a solution-gated FET sensor based on zinc oxide nanorods modified iron oxide nanoparticles (α-Fe_2O_3 NPs) has been reported [17]. The highly conductive solution-gated FET sensor employed the calmodulin (CaM) immobilization on the surface of α-Fe_2O_3–ZnO NRs for selective detection of calcium ions (Ca^{2+}) in the water and serum samples [17]. The fabrication of nozzle-jet printed flexible ZnO nanorods FET glucose biosensor has been reported [18]. Utilization of nozzle-jet printing methods resulted in highly reproducible electrodes with well-defined vertical grown ZnO NRs for high GOx loading and enhanced glucose sensing performance in a wide glucose detection range [18]. A novel FET sensor for HBV DNA diagnosis based on ZnO doped MoS_2 NWs in label free approach was fabricated. The biosensor could detect real samples in sequencing method in high sensitivity. The biosensor could reach to 1 fM LOD at dynamic response time of 25 s the functionality was 96% after eight weeks maintenance [19]. A ZnO-FET, covalently functionalized with single stranded DNA aptamers, provides a highly selective platform for label-free small molecule sensing [20]. The response of the bio-functionalized ZnO-FET was tuned by attaching a redox tag (ferrocene) to the 3′ terminus of the aptamer, resulting in positive current modulation upon exposure to riboflavin down to pM levels [20].

In this paper, a field-effect transistor DNA biosensor based on molybdenum doped ZnO NWs for detecting HBV compatible with complementary metal oxide semiconductor technology in label-free approach was described. In this work, we will show that the fabricated biosensor is potentially suitable for detecting the HBV DNA sequences. The capability of the fabricated biosensor was evaluated by investigating the PCR-verified samples known as True Positive (TP), True Negative (TN), False Positive (FP) and False Negative (FN). The FET biosensor could materialize the clinical tests on samples TP, TN, FP and FN and could distinguish the clinical samples from each other. The designed biosensor showed more precision than the PCR-outcomes by exhibiting more sensitivity on labeled samples known as FN. The DNA target was measured in a linear concentration range from 1 pM to 10 μM. In addition, the FET biosensor showed highly the satisfied specificity for distinguishing serum samples from normal and healthy samples.

2. Experimental details

2.1. Chemicals and materials

The precursors in high purity including molybdenum, zinc metals and sulfur were purchased from Merck Co. (Germany). The silicon wafers (Si; p-type [100]) as substrate were prepared from CGS Co. (Iran). In order to conduct the back-gate measurements and gate modulation and performance, the $K_3Fe(CN)_6/K_4Fe(CN)_6$ at 1 mM concentration in aqueous solution as ionic electrolyte was used. In order to conduct bio-sensing investigations, several samples; 7 positive and 7 negative samples, were materialized. The prepared samples were tested in concentrations ranges from 10 μM to 1 pM. It should be noted that the best concentration in FET biosensing performance in this assay was conducted at 1 nM (maybe due to dynamic pressure and electrostatic geometrical rotation). The oligonucleotides were washed by SD water and kept at −30 °C temperature in the freezer.

2.2. Fabrication of the Mo doped ZnO NWs

In order to grow NWs, first a 150 nm thin layer in thickness was manipulated on p-silicon substrate by magnetron sputtering deposition and controlled by a quartz crystal monitor (thick aligner). The sputtering frequency was 13.56 MHz. The thin films setup fabrication was materialized in two paces; first zinc and then molybdenum were sputtered. The sandwich layer for film materializing was followed: the Mo + Zn 1:9 film was 5 μm in thickness. The growth of the NWs was conducted in the tubular furnace (horizontal and double clamped) at 1600 °C temperature in gas presence (Ar:O_2 ratio 20:1) for 100 min and the outcome was pasted on the FET device for biosensing measurements. It is important to note, until 1000 °C; no oxygen introduction was conducted.

2.3. Fabrication of NWs FET biosensor device

In order to materialize the Mo doped zinc oxide NWs FET device, initially the FET template was prepared. The highly doped p-silicon

(100) type as a back-gate was used as substrate. The FET electrode was comprised by a highly doped Si (p-type) with a SiO_2 thin film (100 nm). The SiO_2 thin layer was served as back-gate terminal. The back gate electrode was used to modulate the charged carriers and their density. Then a 3 μm gold thin film in thickness as electrodes was sputtered on substrate. The source and drain electrodes (Ti/Au (20/60 nm)) were fabricated through electron beam lithography (EBL) with spacing of 300 nm. Prior to the source and drain electrodes defining, the Ti thin film was passivated by sputtering. The FET device was cleansed in ethanol followed by lift-off process. In final step, the Mo doped zinc oxide NWs were pasted on the Au electrodes. In order to optimize Mo doped ZnO NWs FET biosensor, the grown NWs were sonicated in ethanol bath for 1 h, and then the suspension was drop-casted onto the FET electrode. The NWs paste transfer on the FET device was performed under temperature, pressure and wetness control.

In order to characterize the grown NWs morphology and illustrate of Mo doped Zinc Oxide NWs FET surface a field emission scanning electron microscope (FESEM) (Hitachi model: S-4160) and also, for phase determination and crystal investigation a transmission electron microscope (TEM) (model; Philips, CM-30) was applied. For semiconductor measurements, HP4155B SPA the semiconductor parameter analyzer was used at room temperature.

2.4. Preparation of ssDNA probe modified electrode and hybridization process

In order to conduct the FET measurements for NWs electrode; first the NWs electrode surface was prepared in clean room for hindering from bacterial contamination. Then the ss-DNA samples (5 μL; in different concentration) which sonicated in Nafion solution (5 wt %, 10 μL) for 10 min were drop-casted on the electrode surface. In order to remove the non-immobilized ssDNA oligonucleotides; the probe ssDNA modified NWs electrode was dried under argon gas presence at room temperature for 2 h and then gently cleansed with Britton–Robinson (BR) buffer. For performing the hybridization process, the probe electrode was washed with Milli-pore water and rinsed with buffer solution. A hybridized buffer solution was used to hybridize the probe with target. The hybridized buffer solution was 0.5 mM sodium chloride and 0.05 mM sodium citrate. The hybridization process was conducted by drop-casting of the hybridized buffer solution (5 μL) containing target DNA (different concentrations of complementary, non-complementary and mismatches) on the probe modified electrode at room temperature and preserved for 30 min. Then, the NWs/ssDNA/target DNA electrode was washed with BR buffer solution to remove the non-hybridized dsDNA and the FET measurements were implemented. The prepared oligonucleotides samples were prepared in concentrations ranges from 1 pM to 10 μM for ssDNA probe and dsDNA target. It should be noted that the best concentration in FET bio-sensing performance in this assay was conducted at 1 nM (maybe due to dynamic pressure and electrostatic geometrical rotation).

3. Results and discussion

3.1. Biosensor setup and morphological crystal structure characterizations

Fig. 1A and B shows schematically the pre-prepared FET electrode and FET-setup biosensor, respectively (Fig. 1 A and B). Fig. 1A shows the electrode setup in schematic illustration. The drain vs. source spacing distance is around 300 nm. The schematic illustration of the fabricated FET molybdenum doped ZnO NWs biosensor setup is pictured in Fig. 1B. The position of the reference electrode which operates as gate electrode was located on top of bio-sensing setup. The morphology and crystal phase structure characterizations of the fabricated molybdenum doped ZnO NWs were investigated by FESEM and HRTEM microscopic system. Fig. 1C shows the materialized molybdenum doped ZnO NWs morphology on the biosensor electrodes. Fig. 1C shows the molybdenum doped ZnO NWs. The nanoparticles (NPs) which are seen in FESEM image in Fig. 1C were synthesized on the Si substrate. These NPs are Mo doped zinc oxide particles that were not directed well in heat treatment process for NWs fabrication. The geometry of the wire-like (which is validated by TEM and HRTEM images, Fig. 1D) NWs shows that their wide is 50 nm and are several hundred nanometers in length. A large number of the molybdenum doped ZnO NWs are uniformly surfaced on the supporting layer. The well-defined stretched structure of the molybdenum doped ZnO NW was validated by the bright-field TEM image, Fig. 1D. The molybdenum doped ZnO NW was grown by the self-assembly, surface layer by layer and vapor liquid solid growth mechanism. Also they possess perfect sharp edges which brings uniform size of 50 nm with well-defined facets. The HRTEM image (Fig. 1D, inset) shows the spacing facets of the molybdenum doped ZnO NW correspond to (002) plane with the lattice inter-plane spacing of 0.259 nm.

XPS was carried out to investigate the chemical valence states of the different elements and surface elemental composition in Mo doped ZnO. Fig. 2A presents the XPS survey spectrum and shows the presence of Mo, Zn, O, N as well as P in the as-prepared Mo doped ZnO NWs hybridized with DNA sequences sample and their attachment. Fig. 2B presents the Zn 2p spectrum. The peak of binding energy at 1022.3 eV was assigned to Zn $2p_{3/2}$ peak of the Zn^{2+} and at 1044.7 eV was assigned to Zn $2P_{1/2}$ peak of the Zn^{2+}. Metallic Zn with a binding energy of 1021.50 eV was not observed, which confirmed that Zn exists only in the oxidized state. The Mo 3d XPS spectrum (Fig. 2C) showed two peaks at approximately 232.15 eV and 235.25 eV corresponding to Mo $3d_{5/2}$ and Mo $3d_{3/2}$, respectively [19]. Fig. 2D shows the O 1s XPS spectrum, the binding energy at 530.4 eV was assigned to O 1s. As can be seen in the XPS measurements for the NWs sample, noticeable N 1s peak intensity changes were observed at the N 1s peak (Fig. 2E), because of the attachment/interaction of ssDNA with the surface of Mo doped ZnO NWs. In addition, N 1s (401.6 eV) belongs to the amino functionalities in the ssDNA which obviously validates the attachment of ssDNA on the NWs surface. The P 2p XPS spectrum (Fig. 2F) shows the phosphorus attachment on the NWs-ssDNA sample crystal lattice surface.

Fig. 3(A) and (B) shows the transfer and output characteristics of the transistor hepatitis B DNA bio-sensing system at a concentration of 1 nM, respectively. The curve in Fig. 3 (A) shows the transfer characteristics of FP against TN samples. As a comparison view, the overall concept and behavior of the illustrated curves show that these samples have the same bio-sensing electronic behavior. The measured threshold voltage (V_{TH}) for both samples was −4.4 V which calculated by using the square current output slope at $V_{DS} = +1$ V. In the cut-off zone where the value of V_{GS} was less than V_{TH}, no passing current was allowed to exit. When the V_{GS} value was switched from −3 to +1 V, the biosensor graph could have separate linear and saturated areas. The calculated resistance from the linear region at $V_{DS} = +0.5$ V were 404.5 and 98.6 Ω/mm and the bias current in the saturation zone at $V_{DS} = -5$ V was 2.1 and 23.7 mA in applied V_{GS} magnitude of −3 and 0 V, respectively. The fabricated biosensor had low differential current and high resistance in the saturation zone.

Fig. 4 shows the measured output characteristics of the biosensor device for measuring FP samples at different concentrations. In order to evaluate the biosensor response, the single-strand probe was hybridized at low concentrations. It was not expected

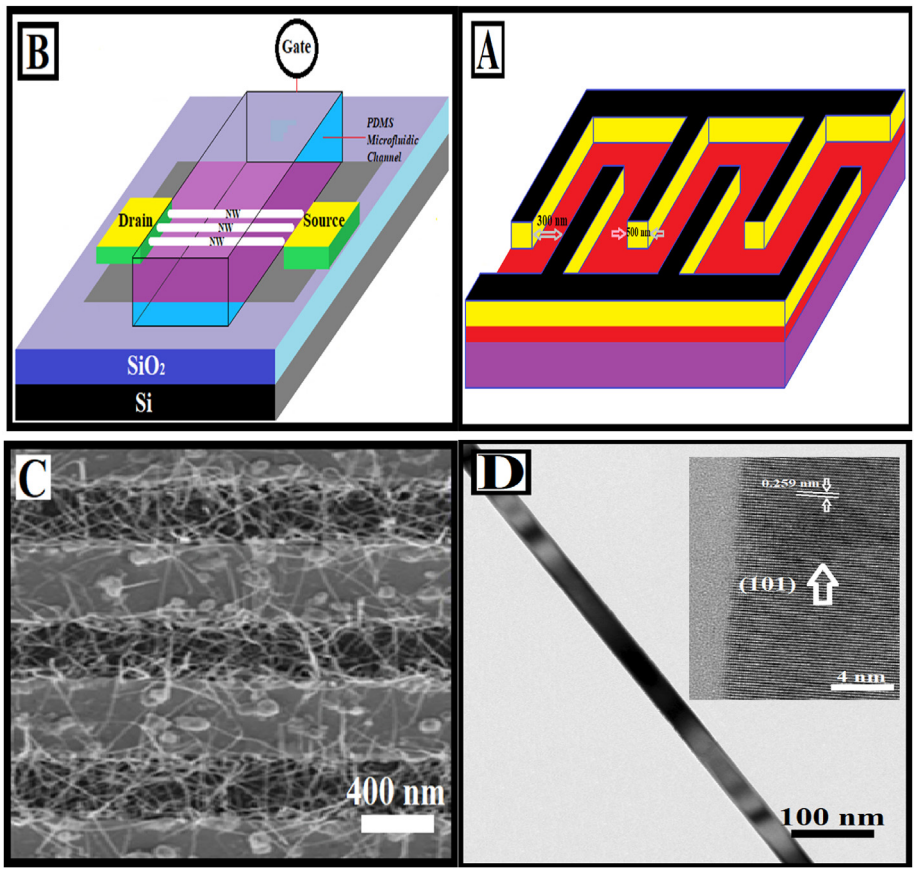

Fig. 1. The morphological and crystal structure characterizations of the fabricated doped ZnO NWs and biosensor setup. (A) The electrode setup in schematic image. The electrode (drain vs. source) spacing distances 300 nm. (B) The schematic picture of the fabricated HBV biosensor setup based on the NWs-FET device. (C) The FESEM image of NWs FET device, scale: 400 nm. (D) The TEM and HRTEM images of the doped ZnO NW with wire like morphological structure.

that the drastic measurement changes during the assay would occur due to the change in threshold voltage (ΔV_{TH}). This process could be materialized, because the HBV DNA biosensor was not operated in open-circuit (from the gate) situation [21]. However, even if the open-gate mode was beneficial for ΔV_{TH}, the severe instability could occur with a biosensor designed in open-circuit mode during the analytical measurements. Therefore, a gate electrode such as the Au layer in this study could be a suitable sensing strategy as backing layer. In addition, the Au surface has been widely developed as a suitable surface for the composition of biomolecules or biomarkers [22]. In order to demonstrate a distinct diagnosis, the measurement strategy was continued from the lowest concentration at 1 pM to the highest concentration at 10 μM. Several functionalized standard analyte solution of FP sample for response measurements with different concentrations of 1 pM, 10 pM, 100 pM, 100 nM, 1 μM and 10 μM were materialized. The chemical stabilization and pairing performance of a single-stranded probe with a complementary target and measuring the hybridization of a single-stranded probe with complementary strand were able to change the forward bias. The biosensor system increased the current output from 2.04 to 3.98 mA for 10 pM and 10 μM before reaching to saturation point, respectively at $V_{DS} = +5$ V reading voltage. In a word, the device was able to achieve the highest surface current as shown in Fig. 3 after modifying the chemical stabilization at the Au gate surface. However, the hybridization of a single-stranded probe with a complementary strand in a FP sample resulted in a regular current decrease. The Huq team also reported that modifying the sensor surface as well as adjusting the Au gate surface enhanced the output current [23]. This bio-sensing mechanism could be explained by the gate surface charge and the concentration of the carrier. The current in the source was regulated by a Schottky gate at the top of the channel. The gating material could change the accumulated charge load, which eventually created bias and changed the biosensor resistance. Finally, the tracking signal from the gate surface was able to enhance the I_{DS} [24]. Therefore, surface charge was the main point in the detection performance, which was the source of current change, was followed by the carrier concentration. To detect concentrations of 1 pM and 10 pM, it could be suggested that there was not enough difference in surface charge or carrier concentration. It was known that an electronic double layer was formed on the metallic gate of the biosensor device [25]. When a single-stranded oligonucleotide was attached to a self-adhesive component of the biosensor, the effective gate dielectric capacity was changed because of the voltage change at the gate electrode. This process could change the corresponding I_{DS}. Typically, no reports of high sensitivity have been reported with a nanowire-based field effect transistor biosensor designed to detect a very small analyte such as DNA [26]. In other words, the identification of large target molecules such as proteins or cells that could easily induce effective capacity changes has been done in the past. In this study, there is no effective difference in the formation of electronic double layers for both of 1 pM and 10 pM. As a point of view on inorganic electron transfer, the thiol group on the nanowire surface in bio-sensing system, which consists of a lethal electron group, could be another source for changing the carrier concentration. According to the group of electrons removed from the oligonucleotide surface, the Au surface has a relatively positive charge. Therefore, a

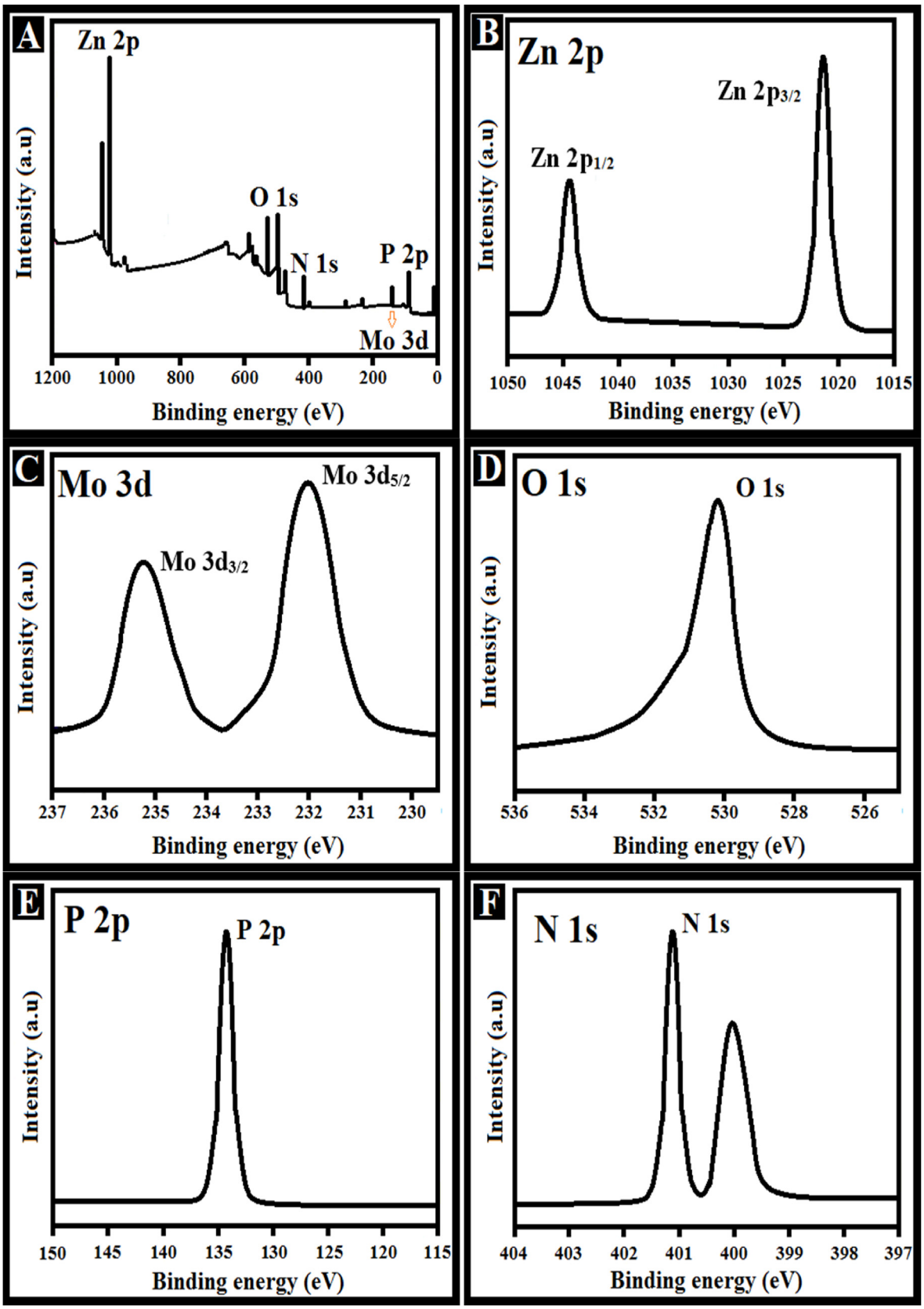

Fig. 2. The XPS survey spectrum (A) and core level spectra of Zn 2p (B), Mo 3d (C), O 1s (D), N 1s (E) and P 2p (F) for DNA hybridized Mo:ZnO NWs.

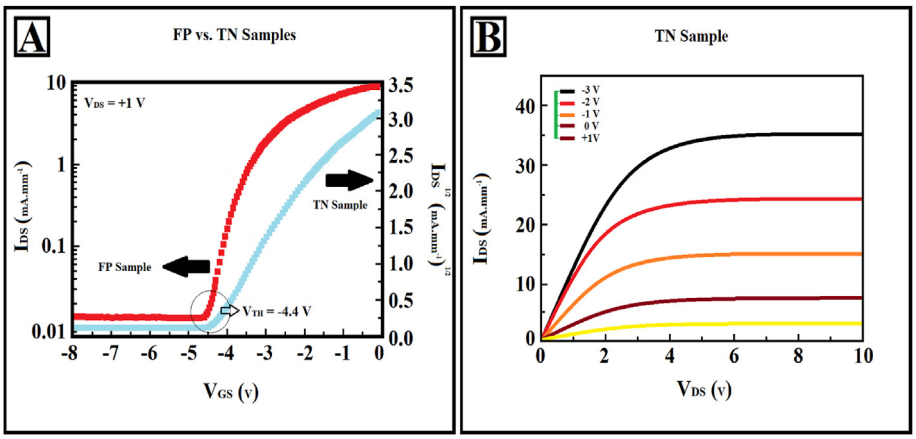

Fig. 3. (A) and (B), the transfer and output characteristics for FET biosensor for hepatitis B DNA, at concentration of 1 nM, respectively.

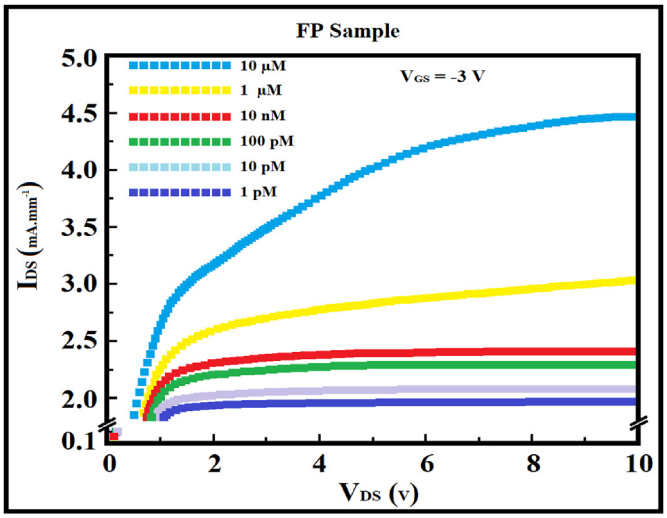

Fig. 4. The calculated output measurements for evaluation of the HBV DNA biosensor response for FP sample at different concentrations of 1 pM, 10 pM, 100 pM, 10 nM, 1 µM and 10 µM.

positively charged surface can induce more two-dimensional electronic gas and increase the drain-source current and forward biased current. In this context, the delay-gate phenomenon is also presented in Fig. 4, and its treatment could be due to the gate surface trap effect. The surface charge of nanowires has been discussed in various studies, which can be easily confirmed with three phenomena: namely, gate leakage current, V_{TH} instability in the transfer curve, and delay-gate in the output curve [27,28]. The system tendency for measuring the analyte sensing can vary according to the structure of the device and effective surface charge. A report on the relationship between the surface charge of a transistor gate and the tendency to single and double-stranded analytes measurement with two different structures has been validly exemplified. In this study, one type shows a tendency to increase the current, while another type shows a tendency to decrease the current, although there is a target modifier for single and double-stranded analytes [25]. Finally, after single-stranded oligonucleotide probe immobilization on the nanowire surface and stabilizing on the surface, the output current was reduced [29]. However, after the single-strand oligonucleotide probe immobilization on the nanowire surface, there was an increase in current, and after hybridizing the complementary target bond and modifying on the surface, the current was decreased [30].

Fig. 5 (A) shows the transfer curve plot for the FP, TN and the healthy samples at a concentration of 1 nM. The designed system could influence the current discharge in the saturation zone under analyte introduction, and increase the output current from 0.4659 mA to 0.4817 mA, which is about 3.39% at the gate voltage with a value of −3 V, see Fig. 5 (A). The current enhancement beyond to saturation situation could be explained by electron erosion in the trap inside the device. The electron trapped inside the (NW + oligonucleotide) system was activated by the excitation voltage and hybridized to the carrier of complementary target which followed by current enhancement. Various studies could investigate the mechanism of trapping in which electron recycling energy has been calculated by Arrhenius equation for electron activation energy [31,32]. Some studies have shown that when the gate voltage was exceeded above the threshold voltage, a photo-electron current would be emitted in the channel region. This photonic energy from the EL emission could have energy band-widths of 1.9 eV and −3.4 eV which ionizes the D_X-D_X-ionized D_X centers. Although the electron current decrease was turned off due to the electron emission factor, ionized D_{Xb} could have been sometimes survived due to the high energy barrier in electron recovery. Finally, this result in stable electron conductivity of the (NW + gate + substrate) buffer layer, led to increase of gate leakage and ultimately loss of environmental status. As shown in Fig. 5B, the threshold voltages (V_{TH}) in the FET biosensor were not affected by the FN and TP samples, while the off-current was about 19.5% and that was increased by the presence of HBV sample compared to healthy conditions in the transfer curve.

Fig. 6 (A) shows the calculated surface current ratios from Figs. 4 and 5 for a TP sample at the lowest concentration and illustrates the current output by detecting different concentrated solutions of the FP sample at different levels. The biosensor current ratio (I_{FP}/I_{TP}) at the reading voltage of +5 V was calculated by measuring of the different concentrated values (1 nM- 1 pM) of the FP and TP samples. The On state in Fig. 6 (A) indicates the state in which the analyte enters and immobilize on the nanowire surface. The off state in Fig. 6 (A) indicates the state that is achieved after washing the electrode surface after the test. The level of the minimum blank value was measured and the LOD parameter of the biosensor was reached at 1 pM. The biosensor device was also able to measure other concentrations of FP sample such as 10 pM, 100 pM and 1 nM. Also, there was no diagnosis based on the current level between 1 pM 1 and 10 pM without On-state. In summary, the biosensor reduced the sensitivity as much as the low concentration of the FP sample to 1 pM and covers the detection range at three orders. As

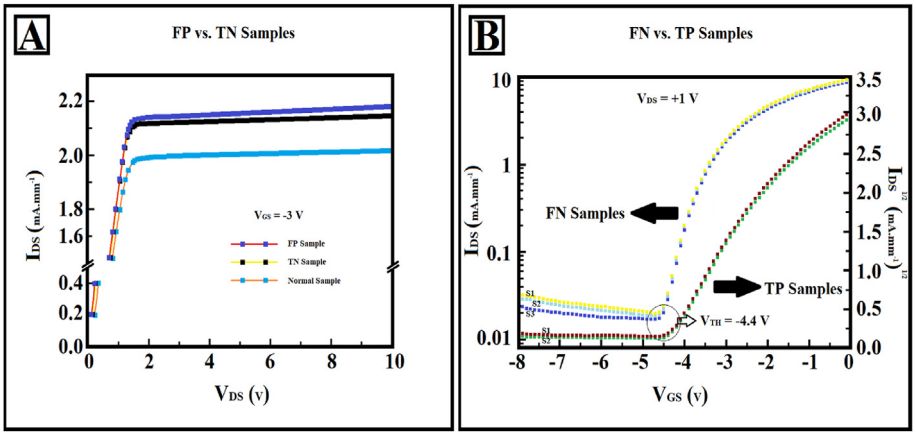

Fig. 5. Characteristics (A) of biosensor output under V_G = - 3V for 3 healthy, false positive and true negative samples. The progressive discharge current in the saturation zone increased from 2.017 mA/mm to 2.164 mA/mm at V_{DS} = + 5V and V_{GS} = - 3V, and characteristics (B) the biosensor transfer under V_G = + 1V for 5 real positive and false negative samples. The leakage current also increased from 0.0174 mA/mm to 0.0208 mA/mm at V_{GS} = - 5V and V_{DS} = +1 V.

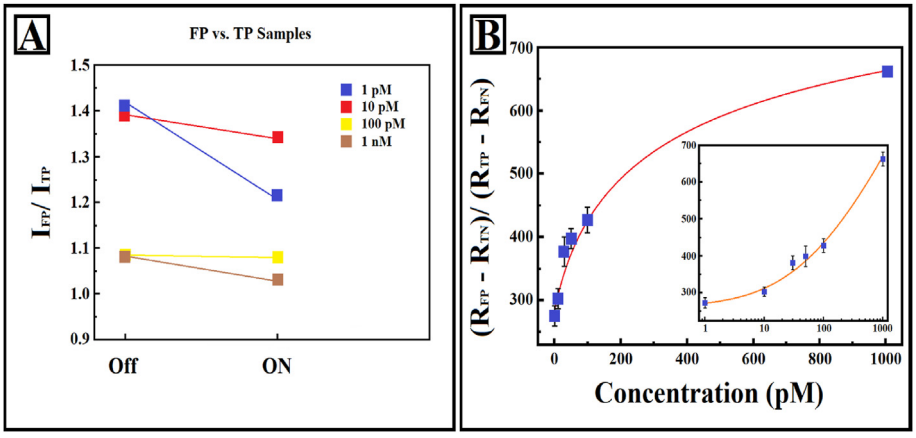

Fig. 6. (A) The calculated surface current ratios from Figs. 4 and 5 for a TN and FT sample at the lowest concentration. (B) The calculated resistance ratios of the samples; (TP), (TN), (FP) and (FN). For a more detailed discussion, (the input diagram in Fig. 6 (B)), Fig. 6 B as a logarithmic concentration scale.

mentioned above, the conduction-activated electron trap increased the carrier concentration, and improves the sensing performance of the nanowire transistor biosensor. Based on present measurements at gate voltage (−3 V), a resistance calibration diagram was calculated. As shown in Fig. 6 (B), the resistance of the samples, (TP), (TN), (FP) and (FN), it has been found [22] that the linearity of normal resistance calibration could minimize changes in biosensor performance depending on fabrication processes or detection protocols, and in addition, normal calibration could be a parameter of accurate design for the measurement membrane which was applied for Real-time measurement [22]. As shown in Fig. 6 (B), even if there was a linear relationship with the least squares method at the low concentration range, the detection ratio after 10 pM was a significant deviation from the linear shape. For more detailed discussion, the input diagram of Fig. 6 (B) was added as the logarithmic concentration scale. As shown in Fig. 6 (B), a reasonable and effective detection of the limited number of probe molecules in the fixed region was available. This means that a high degree of oligonucleotide saturates the molecular sites of the probe at the functional gate, which should result in a nonlinear result or measurement of high concentrations of oligonucleotides. In this case, it is better to dilute the sample further for accurate diagnosis.

Following the commercialization approach, the bio-sensing key was to use the real human sample as well as the standard sample. There were a variety of methods for extracting real samples for human hepatitis B virus DNA from blood. A blood sample from a sick and healthy person was a good option for achieving a non-invasive and rapid method of DNA extraction. In addition, real samples for hepatitis B virus DNA were commonly used as biomarkers of stress and related mental or physical illnesses. Most studies have considered the level of the real sample for hepatitis B virus DNA as a reliable measurement marker for axial adaptation to stress [33]. The initial volume of the samples for clinical trials was the same as volume of a non-clinical samples required for detection and was 5 μl based on PDMS micro-fluidic membrane. Therefore, it could be used immediately for the Care Test System (POCT). Finally, experiments with real sample were performed for 7 cases of true negative, true positive, false positive and false negative human samples after diluting the sample. Fig. 7(A) and (B) and (C) show the calculated ratios of the surface current of the FN sample vs. TN sample at the lowest concentration, the output curve and the transfer curve for 7 TP and FN samples of diluted serum samples, respectively. In Fig. 7 (C) the eighth sample was distilled water. Also the concentration of samples were 1 pM, 10 pM, 100 pM, 10 nM, 1 μ M, 10 μM and 100 μ M and named as S1 to S7 respectively. It should be noted that the FN sample has been selected as a sample of the designed system performance scale in relation to the gold standard. In Fig. 7 (A) the measured current ratio was calculated at

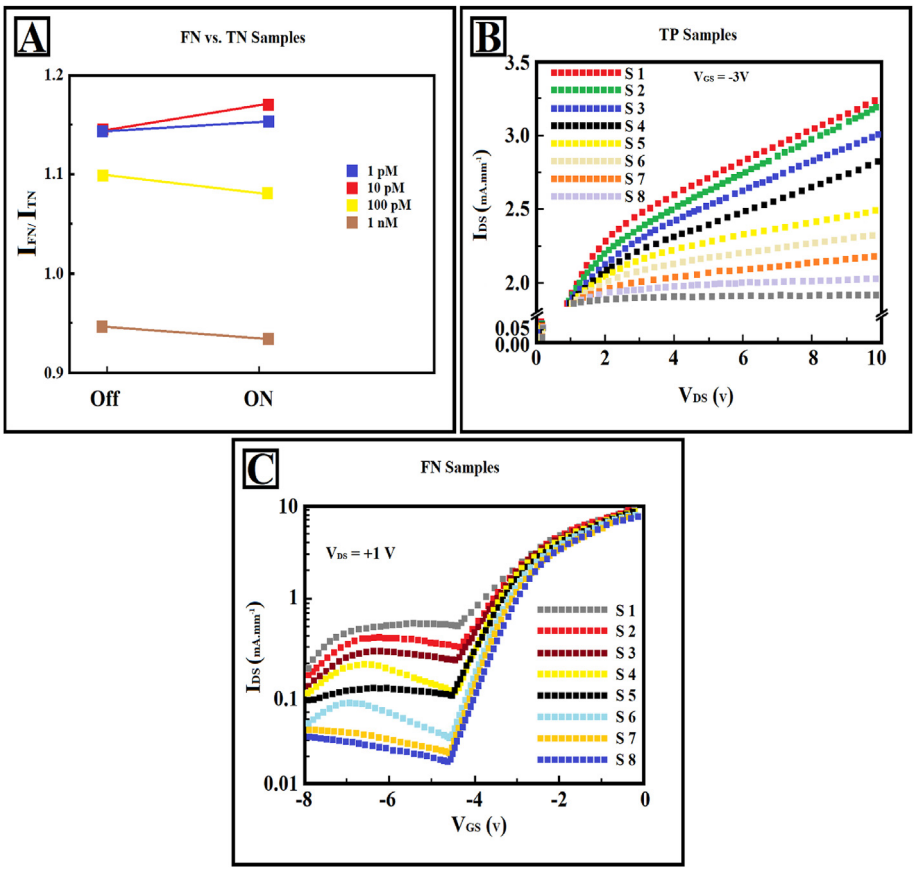

Fig. 7. (A) shows the calculated ratios of the FN sample current rate at concentrations of 1 pM, 10 pM, 100 pM and 1 nM vs. the TN sample. At the lowest concentration, (B) output curve and (C) the transfer curve were diluted for 7 TP and FN samples of serum samples. The samples concentration were 1 p.m., 10 pM, 100 pM, 10 nM, 1 μM, 10 μM and 100 μM, for the sample S1 to S7 respectively.

concentrations of 10 pM, 100 pM and 1 nM as well as the detection limit concentration of 1 pM. The info-diagram clearly shows a high sensitivity of the Mo doped Zinc Oxide NWs electrode. In this case, the detection limit of 1 pM can be evaluated for NWs electrode under electric potential, [19]. The LOD (limit of detection) was estimated via Eq. (1):

$$Y=S_b+3\sigma_b \quad (1)$$

Where S_b is the signal of blank and σ_b is the standard deviation of blank. As shown in Fig. 7 (A), the ratios calculated from the surface current level of the FN sample vs. TN sample at the lowest concentration were illustrated. As shown in Fig. 7 (B), the off-current of the transfer plot, when compared with the margin of the output curve among similar specimens, could show a relatively large margin between different serum samples. In this case, a UV lamp was used to deactivate the vacancy sites, which were created by altering the DTSP without binding the oligonucleotide on the nanowire surface. The strategy and method of virus DNA detection was the same as the standard solution test procedure. In Fig. 7 (C), the biosensor could detect virus DNA at very low dilution for the first time, regardless of the sample type. The transfer curve, which was controlled at a drain voltage $V_{DS} = +1V$, evaluates the behavior of the FN sample in two ways. The first stage is a relatively linear region in which, due to the low DNA of the virus, a relatively small increase in current occurs with increasing voltage. But after the oligonucleotides were aligned, an increase in current occurs after a certain amount of voltage. In addition, the difference between these samples compared to an undiluted sample with a 10 order-diluted serum sample can be discerned (Figs. 6 (A) and 7 (A)). The biosensor has been able to reach a high specifity level for all FN samples. Of the 20 patient samples tested, 7 samples were identified as FN and 7 samples as TP. The designed biosensor was able to detect all of these samples in a different pattern. Since the size of the tested human oligonucleotide was known to be about 1–16 nm [34], it was found that the dilution process was ideal for stable measurement.

In order to evaluate reproducibility of the fabricated FET biosensor, the results for several concentrations were conducted and the relative standard deviation (RSD) values were 2.2%, 3.2%, 2.7% and 2.8% for TN samples at 1 pM, 10 pM, 100 pM and 1 nM concentrations respectively. The resulted RSDs show high accuracy. If the RSD was higher than 9%, the biosensor accuracy would have been lost.

Table .1 shows the comparative study for fabricated biosensor against previous reports on bio-sensing investigations. The fabricated biosensor could prove itself as a significant candidate both in sensitivity and accuracy at bio-sensing technology and science.

4. Conclusion

In this paper, a highly sensitive and easily reproducible FET biosensor based on molybdenum doped ZnO NWs has been materialized. The fabricated biosensor could detect the HBV samples in label-free approach. The FET biosensor conducted the clinical tests on TP, TN, FP and FN and could distinguish the clinical samples from each other. The comparative biosensor showed high sensitivity to samples that the PCR measurements demonstrated

Table 1
The comparison among the reported biosensors.

Sensing technique	Concentration range	LOD	REF.
Fluorometric	**100 pM − 0.040 μM**	**0.05 nM**	[3]
EIS	**0.1 pM to 10 μM**	**1 fM**	[5]
EIS	**0.1 pM to 0.1 μM**	**0.1 fM.**	[6]
ITO-FET	**0.001 pM to 10 μM**	**1 fM**	[7]
MoS2-FET	**0.5 pM to 50 μM**	**1 fM**	[19]
G-FET	**0.5 pM−50 μM**	**0.5 pM**	[35]
LSPR	**$1\times10^{+4}$ pM −100 μM**	**10 nM**	[36]
Fluorometric	**$3\times10^{+6}$ pM−320 μM**	**0.45 nM**	[37]
Fluorometric	**$1\times10^{+5}$ pM−$1\times10^{+3}$ μM**	**24 μM**	[38]
Fluorometric	**$1\times10^{+7}$ pM−0.004 μM**	**4.8 pM**	[39]
G-FET	**$4\times10^{+5}$ pM−50 μM**	**400 nM**	[40]
Mo doped ZnO-FET	**1 pM to 10 μM**	**1 pM**	**This work**

low responsitivity. The FET biosensor showed high accuracy and satisfied specificity by differentiating TP, TN, FP and FN samples from healthy and normal sample in very low LOD and wide concentrations ranges.

CRediT authorship contribution statement

Mohsen Shariati: Conceptualization, Methodology, Data curation, Writing − original draft, Visualization, Investigation, Validation. **Mahdi Sadeghi:** Supervision, Writing − review & editing. **S.H. Reza Shojaei:** Software, Writing − review & editing.

Declaration of competing interest

The authors declare that they have no known competing financial interests or personal relationships that could have appeared to influence the work reported in this paper.

Acknowledgments

The present article is financially supported by “Iran National Science Foundation: INSF” (Project Code: 98017074).

References

[1] B. Negahdari, M. Darvishi, A. Asghar Saeedi, Gold nanoparticles and hepatitis B virus, artificial cells, Nanomedicine, and Biotechnology 47 (2019) 469−474.
[2] Z. Tan, H. Dong, Q. Liu, H. Liu, P. Zhao, P. Wang, Y. Li, D. Zhang, Z. Zhao, Y. Dong, A label-free immunosensor based on PtPd NCs@MoS2 nanoenzymes for hepatitis B surface antigen detection, Biosens. Bioelectron. 142 (2019), 111556.
[3] X. HuiLi, X.L. Zhang, J. Wu, Lin Ni, W.M. Sun, Min Chen, Q.S. Ou, Z.Y. Lin, Hyperbranched rolling circle amplification (HRCA)-based fluorescence biosensor for ultrasensitive and specific detection of single-nucleotide polymorphism genotyping associated with the therapy of chronic hepatitis B virus infection, Talanta 191 (2019) 277−282.
[4] Chun-Yan Yao, Wei-Ling Fu, Biosensors for hepatitis B virus detection, World J. Gastroenterol. 20 (35) (2014) 12485−12492.
[5] M. Shariati, M. Sadeghi, Ultrasensitive DNA biosensor for hepatitis B virus detection based on tin-doped WO_3/In_2O_3 heterojunction nanowire photoelectrode under laser amplification, Anal. Bioanal. Chem. 412 (2020) 5367−5377.
[6] M. Shariati, Impedimetric biosensor for monitoring complementary DNA from hepatitis B virus based on gold nanocrystals, J. Electrochem. Soc. 168 (2021), 016512.
[7] M. Shariati, The field effect transistor DNA biosensor based on ITO nanowires in label-free hepatitis B virus detecting compatible with CMOS technology, Biosens. Bioelectron. 105 (2018) 58−64, 2018.
[8] M. Shariati, The ITO-capped WO_3 nanowires biosensor based on field-effect transistor in label-free protein sensing, Appl. Phys. A 123 (5) (2017) 370.
[9] M. Shariati, S. Alishavandi, Phototransistor properties of indium tin oxide nanowires grown by RF sputtering mechanism and annealing process, Nano 10 (2015), 1550006, 01.
[10] M. Shariati, M. Ghorbani, P. Sasanpour, A. Karimizefreh, An ultrasensitive label free human papilloma virus DNA biosensor using gold nanotubes based on nanoporous polycarbonate in electrical alignment, Anal. Chim. Acta 1048 (2019) 31−41.
[11] M. Shariati, The continuous and persistent periodical growth induced by substrate accommodation in In_2O_3 nanostructure chains and their photoluminescence properties, Appl. Phys. A 118 (3) (2015) 997−1007.
[12] M. Shariati, M. Darjani, The lateral In2O3 nanowires and pyramid networks manipulation by controlled substrate surface energy in annealing evolution, J. Cryst. Growth 436 (2016) 104−112.
[13] M.T. Hwang, M. Heiranian, Y. Kim, S. You, J. Leem, A. Taqieddin, V. Faramarzi, Y. Jing, I. Park, A.M. Van der Zande, S. Nam, N.R. Aluru, R. Bashir, Ultrasensitive detection of nucleic acids using deformed graphene channel field effect biosensors, Nat. Commun. 11 (2020) 1543.
[14] Rafiq Ahmad, Tahmineh Mahmoudi, Min-Sang Ahn, Yoon-Bong Hahn, Recent advances in nanowires-based field-effect transistors for biological sensor applications, Biosens. Bioelectron. V100 (2018) 312−325.
[15] Kiesar Sideeq Bhat, Rafiq Ahmad, Tahmineh Mahmoudi, Yoon-Bong Hahn, High performance chemical sensor with field-effect transistors array for selective detection of multiple ions, Chem. Eng. J. 417 (2021), 128064.
[16] Marya Khan, Mohammad Rizwan Khan, Amal M. Al-Mohaimeed, Tahani Saad Algarni, Ajit Khosla, Rafiq Ahmad, highly sensitive hydrazine detection using a vertically oriented ZnO nanosheet-based field-effect transistor, J. Electrochem. Soc. 167 (2020), 167513.
[17] Rafiq Ahmad, Nirmalya Tripathy, Min-Sang Ahn, Jin-Young Yoo, Yoon-Bong Hahn, Preparation of a highly conductive seed layer for calcium sensor fabrication with enhanced sensing performance, ACS Sens. 3 (2018) 772−778.
[18] Kiesar SideeqBhat, Jin-YoungYoo RafiqAhmad, Yoon-BongHahn, Nozzle-jet printed flexible field-effect transistor biosensor for high performance glucose detection, J. Colloid Interface Sci. 506 (2017) 188−196.
[19] M. Shariati, M. Vaezjalali, M. Sadeghi, Ultrasensitive and easily reproducible biosensor based on novel doped MoS_2 nanowires field-effect transistor in label-free approach for detection of hepatitis B virus in blood serum, Anal. Chim. Acta 1156 (2021) 338360.
[20] Joshua A. Hagen, Sang N. Kim, Burhan Bayraktaroglu, Leedy Kevin, Jorge L. Chávez, Nancy Kelley-Loughnane, Rajesh R. Naik, Morley O. Stone, Biofunctionalized zinc oxide field effect transistors for selective sensing of riboflavin with current modulation, Sensors 11 (7) (2011) 6645−6655.
[21] T. Kokawa, T. Sato, H. Hasegawa, T. Hashizume, J. Vac. Sci. Technol. B, vol. 24, 2006, pp. 1972−1976.
[22] Y.-H. Kim, K. Lee, H. Jung, H.K. Kang, J. Jo, I.-K. Park, H.H. Lee, Biosens. Bioelectron., vol. 98, 2017, pp. 473−477.
[23] H.F. Huq, I. Hector Trevino, J. Castillo, J. Mod. Phys., vol. 7, 2016, p. 1712.
[24] S.J. Pearton, F. Ren, B.H. Chu, Functionalized GaN Bsed Transistors for Biosensing, 2013, pp. 225−251.
[25] J. Yang, P. Carey, F. Ren, Y.-L. Wang, M.L. Good, S. Jang, M.A. Mastro, S.J. Pearton, Appl. Phys. Lett., vol. 111, 2017, 202104.
[26] A. Varghese, C. Periasamy, L. Bhargave, IEEE Sensors, vol. 18, 2019, pp. 747−755.
[27] I. Cimalla, F. Will, K. Tonisch, M. Niebelschutz, V. Cimalla, V. Lebeddev, G. Kittler, M. Himmerlich, S. Krischok, J.A. Schaefer, M. Gebinoga, A. Schober, Friedrich, O. Ambacher, Sensor. Actuator. B Chem., vol. 123, 2007, pp. 740−748.
[28] W. Saito, M. Kuraguchi, Y. Takada, K. Tsuda, I. Omura, T. Ogura, IEEE Trans. Electron. Dev., vol. 52, 2005, pp. 159−164.
[29] B. Lee, J.H. Heo, J.W. Lee, H.H. Cho, J.H. Lee, Sci. Adv. Mater., vol. 11, 2019, pp. 1699−1704.
[30] I. Sarangadharan, A. Regmi, Y.-W. Chen, C.-P. Hsu, P.-C. Chen, W.-H. Chang, G.-Y. Lee, J.-I. Chyi, S.-C. Shiesh, G.-B. Lee, Y.L. Wang, Biosens. Bioelectron., vol. 100, 2018, pp. 282−289.
[31] T.-S. Kang, F. Ren, B.P. Gila, S.J. Pearton, E. Patrick, D.J. Cheney, M. Law, M.-L. Zhang, J. Vac. Sci. Technol. B, vol. 33, 2015, 061202.
[32] T.-S. Kang, Y. Lin, S. Ahn, F. Ren, B.P. Gila, S.J. Pearton, D.J. Cheney, J. Vac. Sci. Technol. B, vol. 34, 2016, 011203.
[33] D.H. Hellhammer, S. Wust, B.M. Kudielka, Psychoneuro 34 (2009) 163−171.
[34] R. Persson, A.H. Garde, Å.M. Hansen, K. €Osterberg, B. Larsson, P. Ørbæk, B. Karlson, Chronobiol. Int. 25 (2008) 923−937.
[35] X. Shicai, Z. Chao, J. Shouzhen, H. Guodong, L. Xiaoyue, Z. Yan, L. Hanping, J. Li, L. Zhenhua, W. Xiaoxin, L. Mingzhen, W. Jihua, Graphene foam field-effect transistor for ultra-sensitive label-free detection of ATP, Sensor. Actuator. B Chem. 284 (2019) 125−133.
[36] L. Xie, X. Yan, Y. Du, An aptamer based wall-less LSPR array chip for label-free and high throughput detection of biomolecules, Biosens. Bioelectron. 53 (2014) 58−64.
[37] W.D. Pu, L. Zhang, C.Z. Huang, Graphene oxide as a nano-platform for ATP detection based on aptamer chemistry, Anal. Methods 4 (2012) 1662−1666.
[38] K. Ma, H. Wang, H. Li, S. Wang, X. Li, B. Xu, W. Tian, A label-free aptasensor for turn-on fluorescent detection of ATP based on AIE-active probe and water-soluble carbon nanotubes, Sensor. Actuator. B Chem. 230 (2016) 556−558.
[39] J. Chen, Y. Liu, X. Ji, Z. He, Target-protecting dumbbell molecular probe against exonucleases digestion for sensitive detection of ATP and streptavidin, Biosens. Bioelectron. 83 (2016) 221−228.
[40] M. Zayats, Y. Huang, R. Gill, C. Ma, I. Willner, Label-free and reagentless aptamerbased sensors for small molecules, J. Am. Chem. Soc. 128 (2006) 13666−13667.